Photoacoustic radio-frequency spectroscopy (PA-RFS): A technique for monitoring absorber size and concentration

Eno Hysi, Dustin Dopsa, and Michael C. Kolios
Department of Physics, Ryerson University, Toronto, Canada
mkolios@ryerson.ca

ABSTRACT

A photoacoustic technique for monitoring absorber size and concentration is presented. The technique relies on analyzing the power spectra of the radio-frequency signals and taking into account the receiving transducer response in order to remove system dependencies. By normalizing the power spectra, parameters derived from ultrasound tissue characterization (spectral slope and midband fit) can be obtained. Tissue mimicking phantoms were constructed using black polystyrene beads of various sizes and concentrations as absorbers. The spectral slope decreased by 0.63 dB/MHz when the size of the particle increased from 1 μm to 10 μm at every bead concentration. The midband fit was ~4 dB higher for the 10 μm particle and increased linearly with concentration. These results suggest that photoacoustic radio-frequency spectroscopy (PA-RFS) can potentially monitor changes in absorber size and concentration thus improving the ability of photoacoustic imaging to distinguish structural tissue variations.

Keywords: Frequency analysis, photoacoustic tissue characterization, power spectra, tissue mimicking phantoms

1. INTRODUCTION

Photoacoustic (PA) images can be reconstructed by displaying the amplitude of the envelope-detected radio-frequency (RF) signals that are received from a passive ultrasound (US) transducer as image brightness pixels. This approach is nearly identical to conventional US B-mode imaging with the exception that the RF signals represent the backscattered echoes formed due to the interactions of the incident US beam with structures within the region of interest (ROI) [1]. The major difference between US and PA imaging is the origin of the RF signals in PA, namely due to the interaction of incident optical irradiation with tissue chromophores (endogenous and exogenous). B-mode US imaging is capable of distinguishing larger-than-wavelength structures because tissue interfaces such as organ boundaries produce well-defined backscattered RF signals thus facilitating the envelope detection process and image formation. This has allowed US imaging to be extended outside of obstetrics into the diagnosis and therapy monitoring of cystic and fibrocystic breast masses as well as other types of carcinoma [2].

US images are degraded by phenomena that are usually not present in other imaging modalities [3]. The degradation of images usually occurs due to the coherent nature of ultrasound and complex spatial distribution of mechanical properties resulting from the internal microstructure of most biological tissues. RF backscattered signals from such structures contain the interference pattern arising from the proximity of the scatterers. These scatterers cannot be resolved in the B-mode images due to overlap in time and this leads to the appearance of speckle [4]. In addition, the speckle in the B-mode images is also affected by the instrument itself as well as the setting used during the exam. The resulting speckle pattern consists of bright and dark spots in the US images that are usually interpreted only on the basis of boundary geometry and texture without providing apparent information about the underlying tissue structure [5]. To overcome these limitations, many investigators have attempted to provide a framework for using US imaging as for quantitative tissue evaluations. These methods described here are commonly referred to as quantitative ultrasound (QUS) techniques are usually based on frequency-domain (spectral) analysis of the backscattered RF signals as opposed to the RF signal envelope [6]–[8]. In this approach, the power spectra of the RF signals from the ROI are first computed. The system dependence is taken into account by computing the power spectrum of the transducer pulse-echo response (typically obtained from a plane reflector) and subtracting it from the power spectrum of the ROI RF signals. This removes the artifacts that are associated with the system transfer function of the electronic transmitter/receiver and the

Photons Plus Ultrasound: Imaging and Sensing 2013, edited by Alexander A. Oraevsky, Lihong V. Wang,
Proc. of SPIE Vol. 8581, 85813W · © 2013 SPIE · CCC code: 1605-7422/13/$18 · doi: 10.1117/12.2004991

operator dependent settings. The resulting spectrum (referred to as the normalized power spectrum) is often quasi-linear over the usable transducer bandwidth (frequency range that has been found to produce adequate signal-to-noise levels).

Linear regression analysis is often performed on the normalized spectrum and several parameters can be extracted. These parameters have been correlated with structural tissue properties and can be used for obtaining quantitative information about the size, shape and concentration of the acoustic scatterers [7]. The spectral slope (SS) of the line of best fit with respect to frequency is an indicator of the effective scatterer shape and size and a decrease in SS corresponds to an increase in the effective scatterer size. Another useful parameter is the midband fit (MBF) which is defined as the value of the regression line at the center frequency of the spectral band. This parameter is numerically equal to the average value of the spectrum over the measurement bandwidth and is a measure of US backscatter that depends on the scatterer size, shape, acoustic impedance and concentration. The spectral analysis techniques relying on the abovementioned parameters have been broadly classified as ultrasonic tissue characterization techniques (UTC) and have proven effective in identifying changes due to the state of prostate, breast and have even been applied for real-time tissue typing [9]. In addition, QUS techniques have been applied to monitoring the morphological changes that occur during chemotherapy treatments of various tumor models [10].

It is well established that in PA, the size of the optical absorber dictates the frequency content of the power spectrum of the RF signals [11], [12]. We postulate that based on this, the spectral analysis of PA RF signals (photoacoustic radio-frequency spectroscopy or PA-RFS) will provide information about the structure of the optical absorber. It is reasonable to expect that information about the size and concentration of the optical absorbers will be manifested in the PA RF power spectra and can be extracted from the SS and MBF parameters of the normalized power spectra. It would be worthy to investigate the potential of PA-RFS for monitoring changes in the size and concentration of PA spherical sources.

2. METHODS

2.1 Phantom construction

Gelatin-based tissue-mimicking phantoms were constructed using black polystyrene beads as spherical absorbers. The gelatin powder was derived from porcine skin (Sigma-Aldrich Co., St. Louis, MO). The two types of black polystyrene beads (Polysciences Inc., Warrington, PA) had an average diameter of 0.9352 ± 0.0276 µm and 10.231 ± 0.344 µm (sizes supplied by the manufacturer). For the purposes of this paper, the sizes of the beads were approximated to 1 µm and 10 µm, respectively. In order to prepare the phantoms, the beads were mixed with degassed water which was heated to ~80 °C prior to adding the gelatin powder. Once the powder was added, the solution was stirred until the entire gelatin had properly dissolved and a homogenous solution had formed. The solution was poured into a phantom mold (4 cm by 4 cm by 2 cm) which was cooled to 4 °C for ~2.5 hours in order to solidify the phantom. For each phantom, 4 g of gelatin powder were mixed with 40 ml of degassed water. For each bead size, three different phantoms were made where the concentration of the beads was changed. Specifically, concentrations of 0.1, 0.2 and 0.3% (v/v) were achieved by mixing the appropriate amount of beads with the degassed water solution prior to heating.

2.2 PA imaging

The Imagio Small Animal PA imaging device (Seno Medical Instruments, Inc., San Antonio, TX) was used to measure all the PA signals analyzed in this study. The system consisted of a Q-switched, pulsed Nd:YAG laser delivered through an articulated arm (beam width 9 mm, pulse width 6 ns, pulse repetition rate 10 Hz, maximum fluence 25 mW/cm2/pulse). The acoustic receiver consisted of a 4 channel, annular array transducer with a center frequency of 5 MHz and a -6 dB bandwidth of 60%, as measured by using a hydrophone as the source of sound. The transducer was mounted 60 mm coaxially to the laser allowing for raster scanning over the entire ROI.

PA signals were recorded from 20 unique locations within each phantom. At each location, the laser fired 4 pulses which were averaged to produce a single PA RF line. In order to obtain the transducer frequency response profile for PA measurements, a 200 nm thick gold film was used. The film was deposited onto a thin microscope cover slide with no annealing. The gold film was used because it has a broad PA power spectrum as well as a flat response in the known bandwidth of the transducer thus providing a good measure of the transducer response in PA measurements. The

laser was raster scanned over an area of ~0.25 cm^2 at 1064 nm using the same power settings as the PA measurements of the phantoms. A total of 20 PA signals were recorded.

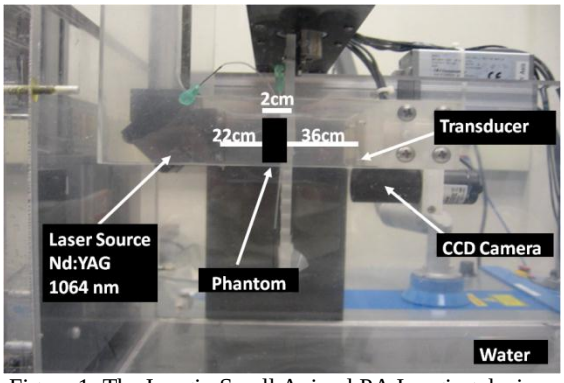

Figure 1: The Imagio Small Animal PA Imaging device.

2.3 Data analysis

The analysis of the entire dataset was performed using Matlab R2009b (The MathWorks, Inc., Natick, MA). Each PA signal recorded was multiplied by a Hamming window in order to localize the signal from the sample as well as minimize spectral leakage. The PA signal amplitude (SA) was calculated by integrating the envelope of each signal (obtained by taking the Hilbert transform). The average SA was then computed by taking the mean of all recorded signals along with the standard deviation for each phantom and the gold film. For each PA signal, the Fourier transform was computed using the Fast Fourier Transform algorithm before converted to a logarithmic (dB) scale.

The power spectra for each RF signal of each phantom were then normalized to the frequency response of the transducer. The normalization procedure was performed by subtracting the gold film spectrum from each power spectrum. Linear regression was performed on the quasi-linear, normalized power spectra over the -6 dB bandwidth of the transducer. The SS and MBF were computed for each spectrum from the linear fit to the normalized spectrum. Averages and standard deviations of each of these parameters were computed. The normality of the data was confirmed using a Shapiro-Wilk test (with $W > 0.05$ used as the criterion for normality). An unpaired t-test was used to compare the PA signal amplitudes and spectral parameters obtained from the 1 μm and 10 μm phantoms for each concentration of beads. A *p*-value of 0.05 or less was used to establish statistically significant differences.

3. RESULTS

The PA signals and the average power spectra for the 1 and 10 μm bead phantoms are shown in figure 2. The PA signals shown in figure 2(a) and figure 2(b) are representative signals from phantoms with 0.3% (v/v) bead concentration. The average power spectra of each phantom are shown in figure 2(c) and the normalized average power spectra are shown in figure 3(d) for 0.3% concentration. The PA signal for the 10 μm bead phantom had higher amplitude than the 1 μm bead phantom. This was reflected in the average power spectra for each phantom where the 10 μm phantom spectral power was significantly higher than the 1 μm bead phantom spectral power across all frequencies. The regression line for the normalized power spectra also showed significantly higher amplitude for the 10 μm phantom and a smaller slope.

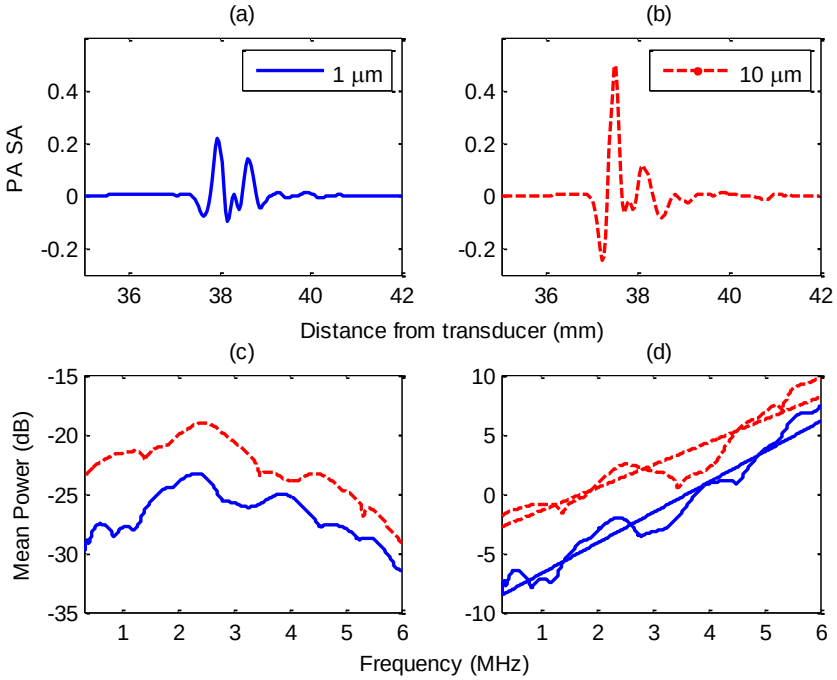

Figure 2: Representative PA signals for (a) 1 μm and (b) 10 μm black polystyrene phantoms along with (c) average power spectra and (d) normalized power spectra and the respective linear fits .The phantoms shown here had a 0.3% (v/v) bead concentration.

The PA SA and spectral parameters (SS and MBF) for all the phantoms constructed for this study are summarized in table 1. For each phantom, the PA SA linearly increased with increasing concentration of beads. The PA SA was ~40% higher for the 10 μm phantom compared to the 1 μm phantom at all concentrations. This change was statistically significant (p = 0.0001). The SS did not change significantly with increasing bead concentration for either phantom. The average value of the SS was 2.55 dB/MHz and 1.92 dB/MHz for the 1 and 10 μm phantoms, respectively. The decrease in SS with increasing bead size was statistically significant for all concentrations (p = 0.0002). Further, the MBF linearly increased with increasing bead concentration for both phantoms. The MBF for the 10 μm phantom was statistically significantly higher than the MBF of the 1 μm phantom at all concentrations (p = 0.002).

Table 1: Summary of the SA and spectral parameters (SS and MBF) for the phantom experiments.

Parameter \ Phantom	1 μm			10 μm		
	0.1%	**0.2%**	**0.3%**	**0.1%**	**0.2%**	**0.3%**
SA (a.u)	0.13 ± 0.2	0.25 ± 0.1	0.49 ± 0.1	0.32 ± 0.1	0.63 ± 0.1	1.27 ± 0.3
SS (dB/MHz)	2.54 ± 0.1	2.55 ± 0.3	2.57 ± 0.3	1.93 ± 0.2	1.90 ± 0.1	1.92 ± 0.2
MBF (dB)	-0.54 ± 0.1	-1.04 ± 0.1	-2.08 ± 0.2	0.52 ± 0.1	1.03 ± 0.1	2.05 ± 0.2

4. DISCUSSION

This study demonstrates the potential of PA-RFS for monitoring the size and concentration of PA sources. The results indicate that the spectral parameters (SS and MBF) are sensitive to changes in size and concentration of the PA sources (black polyethylene beads). Although the relationship between spectral parameters and tissue properties is yet to be determined, the results from this study could be partially interpreted using what is already known from QUS characterizations of tissues [7].

As seen in figure 2 and confirmed from table 1, the increase in the size of the optical absorber (black polyethylene beads) corresponds to an increase in the PA SA and MBF. Theoretical solutions of the wave equation for simple geometries predict that the PA pressure in the frequency domain is proportional to the radius of the absorber squared [13]. This suggests that larger spherical particles will emit PA pressure waves with higher amplitude compared to smaller particles. Such a trend is also observed experimentally since the PA SA for the 10 μm phantom is higher than the 1 μm phantom for all concentrations of beads (figure 2(a) and 2(b)). Furthermore, the trend of PA SA with particle size is also reflected in the MBF spectral parameter as seen by figure 2(d). The MBF increases as the particle size increases and such an increase is in accordance to the increase of PA SA. Specifically, for the 0.3% concentration, the MBF increases by ~4 dB as the size of the particle size increases. This corresponds to an increase in PA SA by a factor of ~2.6. A similar trend was observed for all other bead concentrations. This is in accordance with the relationship that exists between the structural properties of the sample and the MBF parameter as used in UTC. In UTC, an increase in scatterer size results in increased backscatter and thus increased MBF [3]. In PA, it is the size of the absorber that dictates the increase in PA SA and MBF at the frequencies of interest. Despite the fact that the mechanism of US wave generation differs when comparing US and PA, the detection of the backscattered (US) and emitted (PA) signals is identical which suggests that spectroscopic analysis can reveal important information about the sizes and concentrations of PA sources.

As seen in figure 2(d), the SS of the line of best fit to the normalized average spectra decreases as the size of the absorber increases. This trend remains true for all concentrations of absorbers and no statistically significant changes between the SS of varying concentrations for the same absorber size were observed. Specifically, the SS decreases on average by 0.63 dB/MHz when the absorber size increases and the decrease was statistically significant for all 20 PA spectra measured for each concentration. This spectral parameter plays an important role in UTC for monitoring the size of the scatters during the presence of various types of carcinomas as well as during chemotherapeutic treatments of tumors [2], [10], [14]. A decrease in the SS parameter corresponds to an increase in the effective scatterer size. Since the size of the optical absorber dictates the frequency content of the PA power spectra, it is reasonable to expect that changes in PA SS could also be used to monitor changes in the size of the absorber [12]. It should be noted that the transducer bandwidth would significantly affect many of the frequencies generated by the thermoelastic expansion of the optical absorber. By taking into account a transducer with a finite bandwidth, many of the frequencies present in the spectra will be filtered out due to the inherent filtering nature of US transducers [4]. Furthermore, by normalizing the spectra, transducer dependent settings during the measurement can be removed. This provides a set of parameters that can be quantitatively related to tissue properties. The SS parameter computed in this study showed that it is a reliable parameter for monitoring the size of the optical absorber. As seen in table 1, the SS decreased by a factor of ~0.75 when the size of the absorber increased. Such change is significant for successfully monitoring the changes in absorber size given that the concentration of absorber particles was not optimized for the resolution sensitivity of the transducer. In other words, even though the number of beads per resolution volume was not fixed to match the resolution volume of the transducer, analysis of the spectral parameters shows that PA-RFS has the potential to monitor the size and concentration of the optical absorber. Further work is required to determine the exact relationship between the PA spectral parameters and tissue microstructure, especially with regards to the geometry of the vasculature since the RBCs in blood provide the majority of the PA signals *in-vivo* [15].

5. CONCLUSIONS

The results presented here suggest that PA-RFS has the potential to monitor changes in absorber size and concentration. PA-RFS techniques are robust in the sense that they can remove all system dependencies that affect the acquisition of the PA signals and make it difficult to compare studies with different experimental conditions. The method developed here utilizes the spectral content of the PA signals and showed that the SS decreases by ~0.63 dB/MHz as the size of the absorber increased by 10 μm while the MBF increased by ~4 dB. This suggests that PA-RFS is capable of monitoring changes in size and concentration of optical absorbers and can be applied to monitor changes that occur during RBC aggregation.

ACKNOWLEDGEMENTS

This work was made possible due to the financial support of the following granting agencies awarded to M. C. Kolios: Natural Sciences and Engineering Research Council of Canada, Canadian Institutes of Health Research, Canadian

Foundation for Innovation, Canada Research Chairs Program and the Terry Fox Foundation. E. Hysi was supported through the Alexander Graham Bell Graduate Scholarship. A. Worthington is gratefully acknowledged for the technical support. The authors are also very thankful to S. Narasimhan and Y. Wang for their assistance with phantom design.

REFERENCES

[1] J. A. Zagzebski, Essentials of Ultrasound Physics, pp. 1-20, Mosby Inc., St. Louis, MO (1996).

[2] R. M. Golub, R. E. Parsons, B. Sigel, E. J. Feleppa, J. Justin, H. A. Zaren, M. Rorke, J. Sokil-Melgar and H. Kimitsuki, "Differentiation of breast tumors by ultrasonic tissue characterization," J. Ultrasound Med. 12, 601-608 (1993).

[3] F. L. Lizzi, E. J. Feleppa, S. K. Alam and C. X. Deng, "Ultrasonic spectrum analysis for tissue evaluation," Pattern Recogn. Lett. 24, 637-658 (2003).

[4] T. L. Szabo, Diagnostic Ultrasound Imaging: Inside Out, pp. 97-135, Elsevier Academic Press, New York, NY (2004).

[5] F. L. Lizzi, "Ultrasonic scatter-property images of the eye and prostate," Proc. IEEE Ultrasonics Symposium 17, 1109-1117 (1997).

[6] F. L. Lizzi, M. Greenbaum, E. J. Feleppa, M. Elbaum and D. J. Coleman, "Theoretical framework for spectrum analysis in ultrasound tissue characterization," J. Acoust. Soc. Am. 73(4), 1366-1373 (1983).

[7] F. L. Lizzi, M. Ostromogilsky, E. J. Feleppa, M. C. Rorke and M. M. Yaremko, "Relationship of ultrasonic spectral parameters to features of tissue microsctructure," IEEE T. Ultrason. Ferr. 33(3), 319-329 (1986).

[8] E. J. Feleppa, F. L. Lizzi, D. J. Coleman and M. M. Yaremko, "Diagnostic spectrum analysis in ophthalmology: a physical perspective," Ultrasound Med. Biol. 12(8), 623-631 (1986).

[9] E. J. Feleppa, "Ultrasonic tissue-type imaging of the prostate: implications for biopsy and treatment guidance," Cancer Biomark. 4, 201-212 (2008).

[10] M. C. Kolios and G. J. Czarnota, "Potential use of ultrasound for the detection of cell changes in cancer treatment," Future Oncol. 5(10), 1527-1532 (2009).

[11] G. J. Diebold, "Photoacoustic monopole radiation: waves from objects with symmetry in one, two and three dimensions", in Photoacoustic Imaging and Spectroscopy, L. V. Wang, Ed. pp. 3-17, CRC Press, Boca Raton, FL (2009).

[12] A. G. Gertsch, N. L. Bush, D. C. C. Birtill and J. C. Bamber, "Towards characterizing the size of microscopic optical absorbers using optoacoustic emission spectroscopy," Proc. SPIE 7654, 76541M1-10 (2010).

[13] G. J. Diebold, M. I. Khan and S. M. Park, "Photoacoustic signatures of particulate matter: optical production of acoustic monopole radiation," Science 250, 101-104 (1990).

[14] J. Mamou, A. Coron, M. Hata, J. Machi, E. Yanagihara, P. Laugier and E. J. Feleppa, "Three-dimensional high-frequency characterization of cancerous lymph nodes," Ultrasound Med. Biol. 36(3), 361-375 (2010).

[15] J. Zalev and M. C. Kolios, "Detecting abnormal vasculature from photoacoustic signals using wavelet-packet features," Proc. SPIE 7899, 78992M-1-15 (2011).